



POLITECNICO
MILANO 1863

RE.PUBLIC@POLIMI

Research Publications at Politecnico di Milano

Post-Print

This is the accepted version of:

F. Salucci, C.E.D. Riboldi, L. Trainelli, A. Rolando, L. Mariani
A Noise Estimation Procedure for Electric and Hybrid-Electric Aircraft
in: AIAA Scitech 2021 Forum, AIAA, 2021, ISBN: 9781624106095, p. 1-9, AIAA 2021-0258
[AIAA Scitech 2021 Forum, Virtual Event, Jan. 11-15, 19-21, 2021]
doi:10.2514/6.2021-0258

The final publication is available at <https://doi.org/10.2514/6.2021-0258>

Access to the published version may require subscription.

When citing this work, cite the original published paper.

Permanent link to this version

<http://hdl.handle.net/11311/1157662>

A Noise Estimation Procedure for Electric and Hybrid-Electric Aircraft

Francesco Salucci*, Carlo E.D. Riboldi†, Lorenzo Trainelli‡, Alberto Rolando§, and Luca Mariani¶
Politecnico di Milano, Milano, 20156, Italy

In order to quantitatively evaluate the advantages, in terms of noise emissions, of the application of modern electric power-trains to airplanes, an acoustic pollution prediction model was developed. The method mixes the benefits of best-practice and physics-based noise prediction procedures and is applicable to pure-electric and serial hybrid-electric General Aviation aircraft. Numerical results corresponding to circuit patterns in the vicinity of the Milan-Bresso airport are shown, proving the significant noise reduction that flying in pure- or partially-electric mode can bring for light aircraft operating around densely populated areas.

I. Introduction

NEW aircraft pure-electric and hybrid-electric power-trains may bring the most visible effects in the vicinity of airfields, where terminal maneuvers and circuit patterns — the latter typical of training missions — may be flown in pure- or partially-electric mode. Especially for lighter aircraft in the General Aviation (GA) segment, capable of flying in and out smaller airfields often surrounded by densely populated areas, this new capability has the potential to increase public acceptance of near-ground air operations well beyond today's limits.

This in turn can increase the value of such airfields as elements of a diffuse infrastructure for the enhancement of citizens' mobility, for example by assuming a new role as nodes of a short-haul regional air transportation network. This implies the future use of FAR Part 23/CS-23 category commuters, provided with innovative environmentally-sustainable propulsion systems in roles such as the *microfeeder* and the *miniliner*. The former refers to a service for the transfer of passengers to a major hub from scattered aerodromes in the area surrounding it, to avoid longer and less comfortable car traveling, while the latter points to a direct intercity service for commuting passengers, without the need to pass through a hub. Both concepts are among the scope of the EU-funded MAHEPA (Modular Approach to Hybrid Electric Propulsion Architecture) project and UNIFIER19 (Community Friendly Miniliner) project research activities and are documented in [1, 2]. Companion papers [3] and [4] describe market studies that strongly motivate the interest in such smaller-size passenger aircraft developments (see also [5]) and infrastructural studies for the determination of the sizing of the necessary battery-recharging equipment (see also [6]), respectively, providing scenario predictions for the future implementation of a radically new short-haul regional air transportation system.

In order to quantitatively evaluate the advantages of innovative electric propulsion systems, so as to introduce a new performance parameter to be taken into account since an early stage in aircraft design, an acoustic pollution prediction model would be required. Comprehensive models capable of predicting the noise produced by an aircraft considered as a single emitter (instead of an assembly of different noise sources), include best-practice noise prediction procedures from European Civil Aviation Conference (ECAC) [7], which refer to the EUROCONTROL's Aircraft Noise and Performance (ANP) database [8]. Similar procedures are the foundation of such suites as Aircraft Noise Contour (ANCON) [9], FLULA [10], SIMUL [11] and AzB [12]. ECAC procedures [7] provide the means for setting up and validating a comprehensive method of noise prediction, applicable to conventionally-powered aircraft and complying with accuracy standard. Such a method was assumed in this work for the validation of novel estimation procedures. The ECAC model is based on the principle of a standardized discretization of flight maneuvers in proximity to the ground. The discretization resolution is tied to geometric quantities and flight mechanics parameters. The ANP database provides the values of the maximum Sound Pressure Level (SPL) and Sound Exposure Level (SEL), depending on the aircraft power setting and on the slant distance between the noise source and a receiver on ground for several aircraft models and corresponding engine options.

*PhD candidate, Department of Aerospace Science and Technology. AIAA Student Member

†Assistant Professor, Department of Aerospace Science and Technology. AIAA Member

‡Associate Professor, Department of Aerospace Science and Technology. AIAA Member

§Adjunct Professor, Department of Aerospace Science and Technology

¶MSc graduate, Department of Aerospace Science and Technology

II. Proposed estimation approach

In order to build a noise prediction method applicable to aircraft featuring a hybrid-electric power-train, a bottom-up approach was followed. Firstly, suitable noise models for several airplane sub-components were considered, namely: propeller, airframe, thermal engine, gearbox, and electric motor. Inputs for such models include geometrical parameters, quantities describing the flight condition (propeller/thermal engine rotational speed, altitude, flight speed) and environmental conditions (air temperature). Secondly, a global value of the SEL was obtained based on an energetic sum of the contributions from all considered sources, measured through the corresponding SPL values. In order to take into account the inaccuracy of the predictions for these sources, which would yield a highly inaccurate result if simply summed to each other, a source blending method was proposed, where each contribution is weighted by a blending coefficient to be determined. The proposed way of designing the blending coefficients is based on the tuning of the SEL obtained from the sub-component models to match the ANP database data.

The source blending method is based on the following expression for the SEL produced by the aircraft, $L_{E,A}$, as

$$L_{E,A}(d) = 10 \log_{10} \left(\int_{t_1}^{t_2} 10^{x_1 \frac{L_{p,A}^a(d,t)}{10}} + 10^{x_2 \frac{L_{p,A}^p(d,t)}{10}} + 10^{x_3 \frac{L_{p,A}^e(d,t)}{10}} + 10^{x_4 \frac{L_{p,A}^m(d,t)}{10}} + 10^{x_5 \frac{L_{p,A}^g(d,t)}{10}} dt \right), \quad (1)$$

as a function of the slant distance d . The terms appearing in the time-integrated function $L_{p,A}^p(d)$, $L_{p,A}^e(d)$, $L_{p,A}^m(d)$, $L_{p,A}^g(d)$ represent the overall SPL values corresponding to the propeller, engine, electric motor, and gearbox, respectively. In Eq. 1 the energetic sum appears modulated or weighted through a set of *blending coefficients* x_k , $k = 1, \dots, 5$, which, ideally, should all equal 1. As significant uncertainty is associated with the prediction provided by each source, the proposed method provides a way to estimate the blending coefficients in an optimal fashion by minimizing a suitable error cost function. To this end, a set of eight GA single and twin-propeller aircraft in the ANP database were taken as a reference.

The ANP database provides SEL values for a number of aircraft in several weight categories. These were taken as reference values, based on the presumed accuracy of the method. The models for the considered noise sources were applied to the same conditions adopted for obtaining the values in the ANP database. Finally, the blending coefficients were validated by computing the SEL with the proposed source blending method and comparing the results with the output of the ANP database. The complete formulation, including finding the noise models for the sub-components, introducing the source blending method and validating it, is thoroughly discussed in [13].

III. Example noise emission studies

The proposed source-blending prediction method can be deployed to analyze cases of practical interest and, in particular, to investigate the potential of pure-electric and hybrid-electric propulsion in mitigating noise pollution at airports.

The airport of Milan-Bresso (ICAO code: LIMB) has been selected as a test case for quantitative analyses presented herein. This airport is the home base of the Aero Club Milano fleet, which is operated for instructional purposes and for pleasure flights. The fleet is mainly composed of Cessna C172 in several variants and multiple Piper models, including both single-propeller and twin-propeller aircraft. The airport features a single 1 080 m \times 30 m asphalt runway with a 18/36 alignment, and an elevation of 484 ft above sea level. Geographically located at the Northern border of the municipal area of Milan, Italy, the airport is completely surrounded by densely populated districts of the greater Milan area. This feature makes it a critical infrastructure with regards to noise and has fueled an interest in the present analysis.

Based on a realistic description of the circuit around the runway of Milan-Bresso, two analyses are proposed in the present section. First, an assessment of the effect on the noise levels perceived on ground when some or all portions of the circuit are flown in pure-electric mode will be described in detail. To this aim, it will be hypothesized to fly a typical circuit by means of two different conventionally-powered aircraft, i.e. not provided with electric components in the power-plant. Several cases have been analyzed where piston engines are conditionally activated in some clearly identified legs of the circuit. In doing so, as no re-design of the aircraft is taking place, it is implicitly assumed that the necessary battery pack and pure- or hybrid-electric power-plant can be installed on board the existing aircraft without altering its maximum take-off weight and performance requirements. This retrofit can be conveniently evaluated by applying HYPERION, a preliminary sizing tool dedicated to pure-electric and hybrid-electric aircraft design [14, 15]. That said, this comparative analysis produces valuable results to better understand in which parts of the circuit pure-electric propulsion (i.e. the deactivation of piston engines on hybrid-electric power-trains) may have a greater impact in terms of noise pollution.

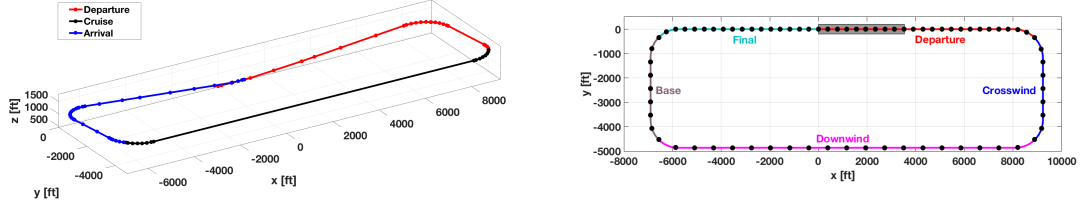


Fig. 1 Geometry discretization (left) and noise sensor placement (right) of the RWY18 right-hand circuit at Milan-Bresso airport.

Subsequently, a comparison is attempted between three existing aircraft, two conventionally-powered ones and a hybrid-electric model currently in an advanced state of development, the Pipistrel Panthera Hybrid, for an assigned circuit trajectory. For the Panthera Hybrid, it is assumed an activation/deactivation strategy for the power generation system (i.e. the system coupling a piston engine with an electric generator that feeds the battery pack and/or the electric motor driving the propeller). This produces very promising results, which highlight the quantitative advantage implied by a fleet switching from aging conventionally-powered models towards new hybrid-electric aircraft in the same weight category and with a similar mission profile.

A. Effect of power-train operational mode

The ECAC modeling approach [7] is applied to the discretization of the right-hand circuit of RWY18, most commonly used in normal operation at Milan-Bresso. The circuit as typically flown by a Cessna 172R aircraft is presented in Figure 1 (left), and features a downwind leg at an altitude of 1 500 ft QNH. It is remarked that the discretization is not only geometrical, but also applies to flight mechanics parameters, as specified by ECAC guidelines. Two aircraft models, the Cessna T206H Stationair and the Piper PA-31-350 Navajo Chieftain, are considered as test-beds.

The prediction of noise emissions is carried out by computing the SEL on an assigned grid of sensors on ground. The source-blending method, with the coefficients computed in [13] can be applied to both aircraft, with the flight trajectory and flight mechanics parameters along the circuit assigned as input.

1. Sound exposure along the circuit ground track

Initially, a grid of sensors is designed along the ground trace of the circuit. The adopted map of sensor points is displayed in Figure 1 (right). This plot also highlights the extension of the five legs in the circuit, namely: departure, crosswind, downwind, base, and final. The positioning of the grid follows the guidelines of ECAC validation scenarios [16]. As typical, the discretization is the result of a compromise between accuracy and computational cost, defined by means of a convergence analysis on the results. The main geometrical data of the grid are reported in Table 1. Clearly, the legs where altitude is changing more rapidly (departure and final) correspond to a finer discretization, whereas the downwind leg, where the aircraft is flying at constant altitude is associated to a looser discretization. The total number of sensors at this stage is 76. It is also worth mentioning that no transient is considered in the adopted noise emission models, so all changes in input and output variables involved in those models (e.g. power settings, rotational speed of the propeller, etc.) take place instantaneously.

As anticipated above, different power management strategies for flying the circuit are considered. Besides the extreme cases represented by using only the piston engine(s) (conventional propulsion case) or only the electric motor (pure-electric case), five further intermediate cases are investigated, as seen in Table 2. In order to present the results of the analysis in a concise form, as looking at the sensors one by one would be impractical, a more comprehensive

Table 1 Grid characteristics for the ground track of the RWY18 right-hand circuit at Milan-Bresso airport.

Leg	Length (on ground) [ft]	Number of sensors	Resolution [ft]
Departure	8 990	24	391
Crosswind	4 360	9	545
Downwind	15 660	21	783
Base	4 370	9	546
Final	6 670	18	392

Table 2 Piston engine conditional activation cases.

ID	Circuit legs with piston engine activated
1	All
2	Departure, Crosswind
3	Departure, Crosswind, Downwind
4	Downwind
5	Downwind, Base, Final
6	Base, Final
7	None

measure is introduced. On account of the energetic nature of the SEL measurement, an energy-based spatial average $\overline{L_E}$ for an arbitrary piece of the ground track trajectory is computed based on the expression

$$\overline{L_E} = 10 \log_{10} \left(\frac{\int_{s_1}^{s_2} 10^{\frac{L_E(s)}{10}} ds}{s_2 - s_1} \right), \quad (2)$$

where the SEL $L_E(s)$ is expressed as a function of the position along a segment of the ground track of the circuit, and s_1 and s_2 correspond to the initial and final extremes of that segment. respectively. By adopting the measurement in Eq. 2 and applying it to each leg in the circuit, it is possible to obtain the results reported in Table 3 and Table 4 for the Cessna T206H and for the Piper PA-31-350, respectively. Both tables display the results of the application of conditional activation strategies for the piston engine listed in Table 2.

At a glance, a comparison of Table 3 and Table 4 points out a generally higher noise for the Piper PA-31-350. This is the result of a larger take-off weight, fuselage size, wing and tail areas, landing gear front section, and of a twin-engine configuration, as opposed to the smaller size and single-engine configuration of the Cessna T206H.

Comparing the legs to one another, it is possible to see that the noise exposure quotas pertaining to departure and final are the highest. For departure, this is the result of a combination of low distance from ground and high power setting. As for the sensors under the final leg, these are exposed to high noise from departure, which justifies the high values of this part (this will be evident from the sound exposure maps in the following).

Considering only the extreme piston engine deactivation strategies, i.e. Cases 1 and 7 in Table 2, it is possible to realize that the sensors under the crosswind leg are associated to SEL values immediately below those pertaining to departure and final, as a result of intermediate power settings and altitudes. Downwind and base are associated to the

Table 3 Average SEL for the Cessna T206H.

ID	Departure [dB]	Crosswind [dB]	Downwind [dB]	Base [dB]	Final [dB]	All legs [dB]
1	93.18	83.22	78.82	76.22	88.92	88.15
2	93.15	83.02	76.44	74.39	88.68	87.99
3	93.16	83.22	78.79	74.82	88.69	88.08
4	90.22	80.45	78.48	74.79	86.21	85.43
5	90.26	80.45	78.52	76.20	86.62	85.55
6	90.26	80.06	75.97	75.89	86.61	85.38
7	90.22	80.06	75.91	74.36	86.20	85.25

Table 4 Average SEL for the Piper PA-31-350.

ID	Departure [dB]	Crosswind [dB]	Downwind [dB]	Base [dB]	Final [dB]	All legs [dB]
1	97.25	87.83	83.19	80.30	91.72	92.03
2	97.22	87.69	80.66	78.66	91.33	91.83
3	97.22	87.83	83.17	78.99	91.34	91.94
4	93.68	85.01	82.96	78.97	88.84	88.87
5	93.75	85.01	82.99	80.29	89.49	89.05
6	93.75	84.73	80.34	80.04	89.47	88.83
7	93.67	84.73	80.29	78.64	88.82	88.65

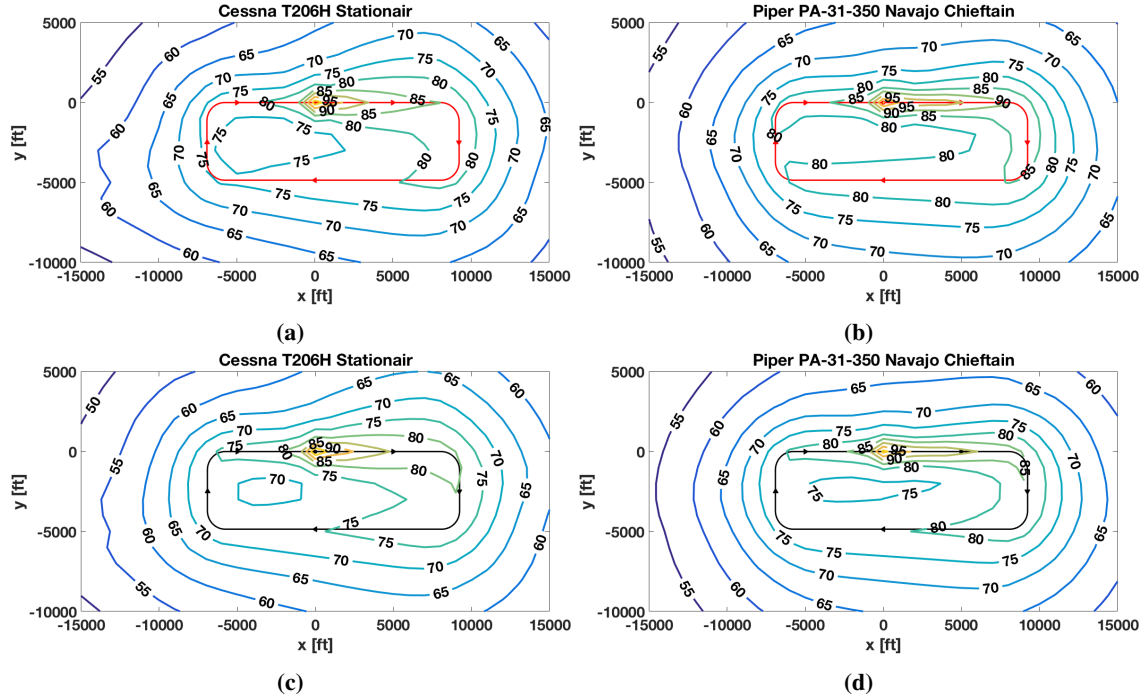


Fig. 2 SEL contour plots (in dB) over an extended sensor grid around Milan-Bresso airport: Case 1 (a) and Case 7 (c) for the Cessna T206H; Case 1 (b) and Case 7 (d) for the Piper PA-31-350.

lowest SEL values, due to a higher distance from ground and lower power settings.

Analyzing the results in terms of conditional activation strategies, it is apparent that the pure-electric (Case 7) and all piston-powered (Case 1) scenarios are associated to the lowest and highest SEL values respectively. Looking at the intermediate cases, it can be seen that SEL values for each leg are roughly polarized around two extreme values. This means that when a leg is flown with the piston engine working, SEL values under that leg assume roughly an extreme, whereas when the piston engine is deactivated, the SEL values are always close to the opposite extreme. This polarization is further confirmed by the similarity between the SEL measures averaged over all legs for the Cases 4, 5, 6, and 7, i.e. when the piston engine is not running or it is run at low power (i.e. on downwind, base and final).

2. Sound exposure over airport area and surroundings

To complement the analysis along the ground track of the circuit, a less refined grid of sensors has been adopted to quantify the SEL on the ground over a more extensive geometrical area. With reference to Figure 1(b), the new sensor grid extends between -15 000 ft and 15 000 ft in the direction of the runway centerline, and from -10 000 ft to 5 000 ft in the cross-centerline direction. The resolution is 1 000 ft in both directions, yielding a total of 496 sensors, which allows to keep computational time to reasonable values.

The SEL contour lines associated to the extreme cases in Table 2 are reported in Figure 2 for the case of both aircraft models under investigation. With the adopted discretization, the computational time for a single plot in this figure is typically between 75 and 90 minutes for the PA-31 and the T206H, respectively, using a single dual-core Intel® Core™ i5 processor.). In order to provide a quantitative description of the noise footprint, Table 5 and Table 6 display the areas A_{nl} contoured by a line corresponding to a given noise level nl (in dB). In both tables, the case ID refers to Table 2. From Table 5, it can be observed that in Cases 1, 2 and 3, when the piston engine is working in the departure and crosswind legs, i.e. at higher regimes, a core of higher noise intensity appears, which especially from Fig. 2(a) can be spotted along the ground track of the circuit, and in particular along the departure leg.

Comparing Cases 1 to 3 with 4 to 7, it can be seen that lower area values are associated to all noise levels for the four latter cases, and the core associated to the highest noise disappears in the same activation scenarios. This supports the results presented above in a more limited framework and is confirmed on the plot in Figure 2(c).

The outcome of the analysis for the twin-engine Piper model is qualitatively similar to that for the Cessna single-

Table 5 SEL contoured areas for the Cessna T206H.

ID	A ₇₀ [ft ²]	A ₇₅ [ft ²]	A ₈₀ [ft ²]	A ₈₅ [ft ²]	A ₉₀ [ft ²]	A ₉₅ [ft ²]	A ₁₀₀ [ft ²]
1	$2.1 \cdot 10^8$	$1.2 \cdot 10^8$	$4.4 \cdot 10^7$	$9.8 \cdot 10^6$	$2.8 \cdot 10^6$	$7.4 \cdot 10^5$	$8.8 \cdot 10^4$
2	$1.8 \cdot 10^8$	$8.9 \cdot 10^7$	$3.8 \cdot 10^7$	$9.6 \cdot 10^6$	$2.7 \cdot 10^6$	$7.2 \cdot 10^5$	$8.4 \cdot 10^4$
3	$2.0 \cdot 10^8$	$1.1 \cdot 10^8$	$4.3 \cdot 10^7$	$9.7 \cdot 10^6$	$2.7 \cdot 10^6$	$7.2 \cdot 10^5$	$8.5 \cdot 10^4$
4	$1.8 \cdot 10^8$	$9.4 \cdot 10^7$	$2.4 \cdot 10^7$	$4.7 \cdot 10^6$	$1.4 \cdot 10^6$	$2.6 \cdot 10^5$	
5	$1.9 \cdot 10^8$	$1.0 \cdot 10^8$	$2.5 \cdot 10^7$	$4.7 \cdot 10^6$	$1.4 \cdot 10^6$	$2.7 \cdot 10^5$	
6	$1.7 \cdot 10^8$	$7.6 \cdot 10^7$	$2.1 \cdot 10^7$	$4.7 \cdot 10^6$	$1.4 \cdot 10^6$	$2.7 \cdot 10^5$	
7	$1.6 \cdot 10^8$	$7.0 \cdot 10^7$	$2.0 \cdot 10^7$	$4.6 \cdot 10^6$	$1.4 \cdot 10^6$	$2.5 \cdot 10^5$	

Table 6 SEL contoured areas for the Piper PA-31-350.

ID	A ₇₀ [ft ²]	A ₇₅ [ft ²]	A ₈₀ [ft ²]	A ₈₅ [ft ²]	A ₉₀ [ft ²]	A ₉₅ [ft ²]	A ₁₀₀ [ft ²]	A ₁₀₅ [ft ²]
1	$2.6 \cdot 10^8$	$1.8 \cdot 10^8$	$9.4 \cdot 10^7$	$2.6 \cdot 10^7$	$7.8 \cdot 10^6$	$2.4 \cdot 10^6$	$3.2 \cdot 10^5$	$3.6 \cdot 10^2$
2	$2.3 \cdot 10^8$	$1.6 \cdot 10^8$	$6.0 \cdot 10^7$	$2.4 \cdot 10^7$	$7.7 \cdot 10^6$	$2.3 \cdot 10^6$	$3.0 \cdot 10^5$	$1.9 \cdot 10^2$
3	$2.5 \cdot 10^8$	$1.7 \cdot 10^8$	$8.8 \cdot 10^7$	$2.6 \cdot 10^7$	$7.7 \cdot 10^6$	$2.4 \cdot 10^6$	$3.0 \cdot 10^5$	$2.0 \cdot 10^2$
4	$2.3 \cdot 10^8$	$1.6 \cdot 10^8$	$7.4 \cdot 10^7$	$1.3 \cdot 10^7$	$3.7 \cdot 10^6$	$6.1 \cdot 10^5$	$3.2 \cdot 10^4$	
5	$2.4 \cdot 10^8$	$1.7 \cdot 10^8$	$7.9 \cdot 10^7$	$1.4 \cdot 10^7$	$3.8 \cdot 10^6$	$6.6 \cdot 10^5$	$3.8 \cdot 10^4$	
6	$2.1 \cdot 10^8$	$1.4 \cdot 10^8$	$4.9 \cdot 10^7$	$1.3 \cdot 10^7$	$3.8 \cdot 10^6$	$6.6 \cdot 10^5$	$3.7 \cdot 10^4$	
7	$2.1 \cdot 10^8$	$1.4 \cdot 10^8$	$4.5 \cdot 10^7$	$1.2 \cdot 10^7$	$3.7 \cdot 10^6$	$6.1 \cdot 10^5$	$3.2 \cdot 10^4$	

engine aircraft. As observed, the configuration of this Piper model is forcibly associated to higher noise emissions than the Cessna aircraft. This is testified by the appearance of a top noise core associated to 105 dB in Table 6, whereas the corresponding value in Table 5 amounts to 100 dB. The generally more intense noise emission of the Piper PA-31-350 is testified also by the larger areas corresponding to the same SEL level, as can be seen from the comparison of corresponding columns on Table 5 and Table 6. This has a match in the stretched shapes of contoured areas associated to the highest noise levels in the (b) and (d) plots of Figure 2, pertaining to the Piper aircraft. By comparison, the contoured areas associated to the highest noise levels for the Cessna ((a) and (c) plots) are clearly more compact.

B. Effect of different propulsion systems

After assessing the effect of different piston engine activation strategies, without altering the actual structure of two existing conventionally-powered aircraft, an analysis is attempted on three more realistic test-beds.

Three aircraft models have been selected for the purpose: two are representative of conventionally-powered General Aviation 4-seaters, the vintage Cessna C172R Skyhawk and the modern Pipistrel Panthera; the third is the novel hybrid version of the latter, the Pipistrel Panthera Hybrid, that is currently being developed under the MAHEPA (Modular Approach to Hybrid Electric Propulsion Architecture) project.

Again, the case of the RWY18 right-hand circuit of Milan-Bresso airport has been considered. As pointed out, the computation of sound exposure is based on the definition of a segmented aircraft trajectory and on the creation of a set of NPD data, made according to the source-blending method. The behavior of the flight mechanics parameters along the trajectory of the circuit has been simulated following the guidelines of the ANP database, starting from the data listed for a Cessna C172R. The guidelines have been emended considering the actual circuit altitude of the considered circuit.

For the case of the Pipistrel Panthera in both its configurations, not included in the database, the same trajectory of the Cessna C172R has been assumed. Due to a general similarity in size, weight, and power, this assumption is considered reasonable. The aforementioned altitude limitations due to regulations over Milan-Bresso further reduce the impact of such assumption – actually, all aircraft operating from this airport fly a very similar circuit trajectory. It also brings in as a plus the chance to assess differences in emissions only due to aircraft-specific features, and not to differences between trajectories.

Concerning noise emissions, the blending coefficients have been identified and adopted for all aircraft considered. For the case of the Panthera Hybrid, propelled by a series-hybrid power-train, it has been assumed that the propeller is always driven by the brushless Siemens e-Motor SP150D. The power trend with respect to rotational speed is assumed linear, so that shaft power is directly proportional to rotational speed.

In order to keep as close as possible to a realistic scenario, the Panthera Hybrid circuit flight has been analyzed assuming to activate the piston engine, a Rotax 914, only when the aircraft reaches the maximum allowable altitude, as

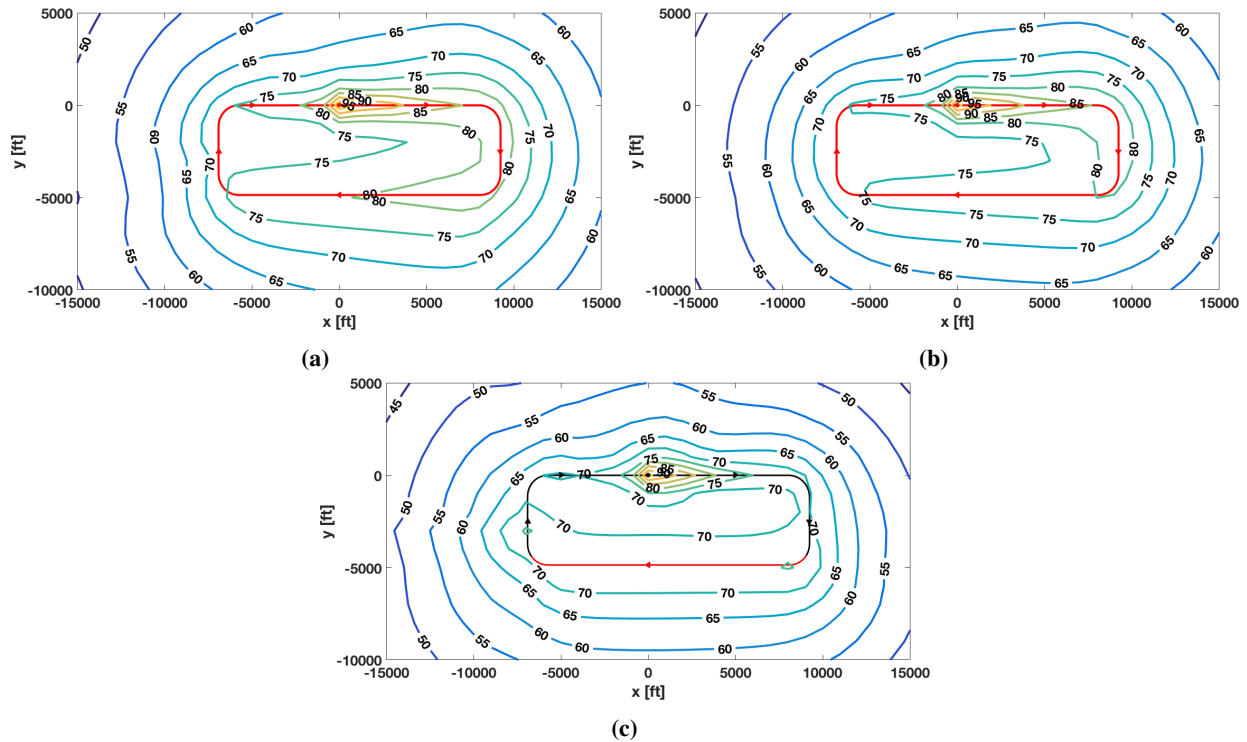


Fig. 3 SEL contour plots (in dB) over an extended sensor grid around Milan-Bresso airport: Cessna C172R Skyhawk (a), Pipistrel Panthera (b), Pipistrel Panthera Hybrid (c).

operationally prescribed. In turn, this roughly corresponds to an engine activation along the downwind leg. Clearly, the two conventionally-powered aircraft are analyzed with the piston engine always running.

The SEL contour plots, computed on the same grid considered previously, are presented in Figure 3. As pointed out, from the three plots in Figure 3, it can be noted that the most intense SEL values are recorded in proximity to the departure leg, as this is characterized by the highest power settings and the lowest slant distances between the aircraft and the receiver on ground. The higher intensity of emissions in this phase is also responsible for relatively high SEL values on the ground track of the final leg. By comparison, the higher distance from ground typical of the downwind leg, and the lower power settings of the base and final (the latter with the caveat just mentioned), are associated to a generally lower noise mark on ground for these legs.

Comparing the plots pertaining to the two conventional aircraft, these are qualitatively similar, but a difference in the extreme values can be noticed far from the circuit, especially part of the aircraft along the downwind leg, showing a generally lower noise footprint for the Panthera. Inside the circuit (i.e. in the immediate vicinity of the runway and aerodrome area) more significant differences can be appreciated in the shapes of the contour plots, but the values of the SEL are generally similar for both aircraft.

The Panthera Hybrid case displays some marked differences with the other two cases. Looking at the regions out of the circuit, the SEL is generally significantly lower for this aircraft, especially closer to high-power legs (departure, crosswind). It can be noticed also that the SEL gradient along the departure leg is more pronounced for the hybrid-electric case. Looking at the downwind leg, the activation of the piston engine at maximum regime in this phase produces a 70 dB contour line parallel to the downwind leg, which contrasts with the noise intensity decay registered for the two conventional airplanes.

To quantitatively compare the results in Figure 3, the same approach adopted for Table 5 and Table 6 has been adopted in Table 7 for the three aircraft considered in this phase. Considering in a first stage the two conventionally-propelled models, it can be noticed that, somewhat unexpectedly, sound exposures higher than 100 dB are produced by the conventional Panthera, which is also associated to the largest contoured areas for SEL values of 85 dB and above, i.e. performing somewhat worse than the older C172R. Looking at the emission maps in Figure 3, such effect is likely due to the take-off phase, as exposures higher than 85 dB are registered only near the departure leg. A possible explanation

Table 7 SEL contoured areas for the Cessna C172R Skyhawk, Pipistrel Panthera, and Pipistrel Panthera Hybrid.

Aircraft	A ₇₀ [ft ²]	A ₇₅ [ft ²]	A ₈₀ [ft ²]	A ₈₅ [ft ²]	A ₉₀ [ft ²]	A ₉₅ [ft ²]	A ₁₀₀ [ft ²]
Cessna C172R	$1.9 \cdot 10^8$	$1.1 \cdot 10^8$	$3.4 \cdot 10^7$	$6.2 \cdot 10^6$	$1.9 \cdot 10^6$	$2.5 \cdot 10^5$	
Pipistrel Panthera	$1.8 \cdot 10^8$	$9.0 \cdot 10^7$	$2.8 \cdot 10^7$	$7.4 \cdot 10^6$	$2.6 \cdot 10^6$	$6.0 \cdot 10^5$	$1.6 \cdot 10^4$
Pipistrel Panthera Hybrid	$7.9 \cdot 10^7$	$8.3 \cdot 10^6$	$4.1 \cdot 10^6$	$1.9 \cdot 10^6$	$5.5 \cdot 10^5$	$9.0 \cdot 10^3$	

for this effect is linked to Dobrzynski’s model for piston engine noise [17], which accounts only for maximum power and not for its actual value. The conventional Panthera version is equipped with a 260-hp Lycoming IO-540-V, which is much more powerful than the Lycoming IO-360-L2A installed on the Cessna C172R Skyhawk. This results into a generally higher engine noise, and consequently also a larger exposure for the conventional Panthera during take-off and climb, i.e. two phases in which the contribution of the engine is mostly relevant.

On the other hand, the areas relative to the lower SEL values are higher for the Cessna C172R Skyhawk than the conventional Panthera (e.g. the 80 dB and the 75 dB lines). Looking at the emission maps in Figure 3, this difference is associated with a different behavior in the first part of the downwind leg, and may be related to the landing gear contribution to the overall aircraft noise. As engine power is not at its maximum value over this leg, the engine and propeller noise emission levels are comparable to the airframe contribution, in turn mainly related to landing gear, greater than wing noise level and for a flap deflection assumed null. Considering the Panthera, landing gear retraction has been assumed in the generation of the NPD data adopted for this flight phase, whereas the Cessna C172R Skyhawk is equipped with a fixed landing gear, contributing to the difference in overall aircraft noise. Focusing now on the Panthera Hybrid, the lower contoured areas in Table 7 confirm the generally lower noise footprint of this aircraft, as observed. There are also in this case locations where the SEL reaches 95 dB, but the corresponding contoured area is two orders of magnitude smaller than the value pertaining to the Cessna C172R Skyhawk and conventional Pipistrel Panthera. The region contoured by the 90 dB and the 85 dB contour lines is three-times smaller for the Panthera Hybrid with respect to Cessna C172R Skyhawk, as a result of the different gradient in proximity to the departure leg, as observed. The area enclosed by the 85 dB line for the Panthera Hybrid roughly matches that associated to the 90 dB level for the Cessna C172R Skyhawk.

Considering the lowest exposure levels, a more interesting comparison is made with respect to the conventional Panthera, associated to lower values than the Cessna C172R Skyhawk. Looking at the 75 dB and 80 dB levels, the corresponding enclosed region is one order of magnitude larger for the conventional Panthera than for its hybrid-electric version. Since the aerodynamic and structural characteristics are the same for the two aircraft, such behavior is due to the effect of the electric component of the power-train.

On the other hand, the area contoured by the 70 dB contour line for the case of the Panthera Hybrid is only 2.2 times smaller than the corresponding value for the conventional version, as a result of the large 70 dB area produced on both sides of the downwind leg, as noted in Figure 3(c).

IV. Conclusion

The present paper presents results from a new practical procedure to predict the noise produced and propagated by an aircraft featuring a novel pure- or hybrid-electric power-train in the vicinity of an airport. The procedure is applied to two case studies, both set in the the circuit around the Milan-Bresso city airport. In the first case, the effect of the various activation strategies of a fuel-burning power generation system is taken into account, demonstrating the efficacy of some of such strategies in significantly reducing the noise perceived on the ground. Ideal hybridized variants of two existing aircraft have been introduced for testing in this study. In the second example, a contrast is made between existing conventionally-powered aircraft and the Pipistrel Panthera Hybrid, a hybrid-electric aircraft currently in an advanced development stage. In terms of noise reduction, the ability of the hybrid-electric architecture is clearly demonstrated, thus quantitatively documenting the gain provided by this novel type of power-trains and confirming the ability of the proposed noise estimation approach through sensible results.

Acknowledgments

The research leading to the presented results has received funding from Project MAHEPA, financed by the EU H2020 Programme under Grant Agreement N. 723368.

References

- [1] Erzen, D., Oliviero, F., and Trainelli, L., “Conceptual Design of a Near-Zero Emission and Cost-Efficient Regional Air Mobility Solution,” *10th EASN International Conference*, September 2–4, 2020.
- [2] Rolando, A., Salucci, F., Trainelli, L., Riboldi, C. E. D., and Khan, Y. M., “On the Design of an Electric-Powered Micro-Feeder Aircraft,” *1st Aerospace Europe Conference (AEC 2020)*, Bordeaux, France, February 25–28, 2020, pp. 1–11.
- [3] Salucci, F., Trainelli, L., Bruglieri, M., Riboldi, C. E. D., and Rolando, A., “Capturing the Demand for an Electric-Powered Short-Haul Air Transportation Network,” *AIAA SciTech 2021 Forum*, January 11–15, 2021.
- [4] Salucci, F., Trainelli, L., Riboldi, C. E. D., and Rolando, A., “Sizing of Airport Recharging Infrastructures in Support to a Hybrid-Electric Fleet,” *AIAA SciTech 2021 Forum*, January 11–15, 2021.
- [5] Trainelli, L., Riboldi, C. E. D., Rolando, A., and Salucci, F., “Methodologies for the Initial Design Studies of an Innovative Community-Friendly Miniliner,” *IOP Conference Series: Materials Science and Engineering*, 2021. Accepted.
- [6] Salucci, F., Trainelli, L., Faranda, R., and Longo, M., “An optimization Model for Airport Infrastructures in Support to Electric Aircraft,” *2019 IEEE Milan PowerTech*, Milan, Italy, June 2019, pp. 1–5. <https://doi.org/10.1109/PTC.2019.8810713>.
- [7] ECAC, *Report on standard method for computing noise contours around civil airports - Volume 2: Technical Guide*, Neuilly-sur-Seine, France, 2016.
- [8] EUROCONTROL, *The Aircraft Noise and Performance (ANP) database: an international data resource for noise modellers*, 2006. URL www.aircraftnoisemodel.org.
- [9] Ollerhead, J. B., Rhodes, D. P., Viinikainen, M. S., Monkman, D. J., and Woodley, A. C., “The UK Civil Aircraft Noise Contour model ANCON: Improvements in Version 2.” Tech. Rep. 9842, NATS, 1999.
- [10] Pietrzko, S., and Bütikofer, R., “FLULA - Swiss Aircraft Noise Prediction Program,” *Acoustics 2002 Innovation in Acoustic and Vibration.*, Adelaide, Australia, November 13–15, 2002.
- [11] Isermann, U., Matschat, K., and Müller, E. A., “Prediction of Aircraft Noise Around Airports by a Simulation Procedure,” *Inter-Noise 86*, Cambridge, MA, July 21–23, 1986, pp. 717–722.
- [12] Deutsche Umweltbundesamt, *Anleitung zur Berechnung von Larmschutzbereichen (AzB)*, 2007. URL www.hlnug.de.
- [13] Riboldi, C. E. D., Trainelli, L., Mariani, L., Rolando, A., and Salucci, F., “Predicting the effect of electric and hybrid-electric aviation on acoustic pollution,” *Noise Mapping*, Vol. 7, No. 1, 2020, pp. 35–56. <https://doi.org/10.1515/noise-2020-0004>, URL <https://www.degruyter.com/view/journals/noise/7/1/article-p35.xml>, publisher: De Gruyter Section: Noise Mapping.
- [14] Riboldi, C. E. D., Gualdoni, F., and Trainelli, L., “Preliminary Weight Sizing of Light Pure-Electric and Hybrid-Electric Aircraft,” *Transportation Research Procedia*, Vol. 29, 2018, pp. 376–389.
- [15] Trainelli, L., Riboldi, C. E., Salucci, F., and Rolando, A., “A General Preliminary Sizing Procedure for Pure-Electric and Hybrid-Electric Airplanes,” *1st Aerospace Europe Conference (AEC 2020)*, Bordeaux, France, February 25–28, 2020, pp. 1–10.
- [16] ECAC, *Report on standard method for computing noise contours around civil airports - Volume 3: Reference Cases and Verification Framework*, Neuilly-sur-Seine, France, 2016.
- [17] Bertsch, L., Dobrzynski, W., and Guerin, S., “Tool development for low-noise aircraft design,” *Journal of Aircraft*, Vol. 47, No. 2, 2010, pp. 694–699.